Optics Letters

Topological effects in anisotropy-induced nano-fano resonance of a cylinder

Dongliang Gao,[1,2] Lei Gao,[1,2,*] Andrey Novitsky,[3] Hongli Chen,[1] and Boris Luk'yanchuk[4]

[1]College of Physics, Optoelectronics and Energy of Soochow University, and Collaborative Innovation Center of Suzhou Nano Science and Technology, Soochow University, Suzhou 215006, China
[2]Jiangsu Key Laboratory of Thin Films, Soochow University, Suzhou 215006, China
[3]Department of Theoretical Physics and Astrophysics, Belarusian State University, Nezavisimosti Avenue 4, 220030 Minsk, Belarus
[4]Data Storage Institute, DSI Building, 5 Engineering Drive 1, Singapore 117608, Singapore
*Corresponding author: leigao@suda.edu.cn

Received 5 June 2015; revised 26 July 2015; accepted 28 July 2015; posted 11 August 2015 (Doc. ID 242429); published 1 September 2015

We demonstrate that optical Fano resonance can be induced by the anisotropy of a cylinder rather than frequency selection under the resonant condition. A tiny perturbation in anisotropy can result in a giant switch in the principal optic axis near plasmon resonance. Such anisotropy-induced Fano resonance shows fast reversion between forward and backward scattering at the lowest-energy interference. The near and far fields of the particle change dramatically around Fano resonance. The topology of optical singular points and the trajectory of energy flux distinctly reveal the interaction between the incident wave and the localized surface plasmons, which also determine the far-field scattering pattern. The anisotropy-induced Fano resonance and its high sensitivity open new perspectives on light–matter interactions and promise potential applications in biological sensors, optical switches, and optomechanics.

OCIS codes: (160.1190) Anisotropic optical materials; (240.6680) Surface plasmons; (290.4020) Mie theory; (290.5825) Scattering theory.

http://dx.doi.org/10.1364/OL.40.004162

Light scattering by a small particle is one of the most fundamental problems in electrodynamics and has potential applications in information processing, nanotechnologies, and engineering. For particles with a size much smaller than the incident wavelength, Rayleigh approximation can be adopted [1]. Nonetheless, recent studies show that, for a small particle with weak dissipation frequencies, anomalous light scattering takes place near plasmon resonance with unexpected features, e.g., sharp giant optical resonances with inverse hierarchy [2] and an asymmetric scattering profile [3,4]. These unusual properties are typical Fano resonances that originate from the constructive and destructive interference of a discrete plasmon with a continuum incident light [5,6]. The interference also can bring up various interesting phenomena such as handedness inversion of optical vortex [7], optical second-harmonic generation [8], Fano-induced optical force [9,10], etc. Fano resonance has promising applications in biological sensor, plasmonic switch [11], and engineering nanostructures [12]. Recently, a lot of studies were related to the resonances in plasmonic nanostructures [3,4,13], coherent nanocavities [14], and metallic films [15]. Asymmetric structures were intensively used to manipulate the coupling between different plasmon modes [16–18]. However, they were focused on isotropic materials or elements, and Fano resonances were observed versus the fine-tuning of a frequency.

Similar to the breaking of the structure symmetries, introducing anisotropy into the system could not only show the generic effect of singular optics, such as conservation of topological index and charge [19], but also render possibilities in plasmonic manipulation and nonlinear photonics. In this Letter, we provide a new paradigm to realize Fano resonance via the anisotropy of a single particle instead of controlling frequency. This novel resonant mechanism may be a new approach for sensitive optical identification of molecular groups, calculation of heating, radiation pressure, and trapping. The anisotropy is found to be able to tailor the surface plasmon resonance and induce additional plasmonic resonances. Thus, this Letter reveals that anisotropy-induced Fano resonance occurs to the anisotropic rod, and its radiation pattern is affected by the subtle perturbation of the rod's anisotropy. We also look into the near field where Poynting bifurcation and vortex analysis [20] are investigated against the anisotropy-induced Fano resonant cases.

Here, we consider a homogeneous rod in air with radial anisotropy in both $\overleftrightarrow{\varepsilon}$ and $\overleftrightarrow{\mu}$; the constitutive tensors of the relative permittivity and permeability are expressed as $\overleftrightarrow{\varepsilon} = \varepsilon_r \overleftrightarrow{r}\overleftrightarrow{r} + \varepsilon_\theta \overleftrightarrow{\theta}\overleftrightarrow{\theta} + \varepsilon_z \overleftrightarrow{z}\overleftrightarrow{z}$ and $\overleftrightarrow{\mu} = \mu_r \overleftrightarrow{r}\overleftrightarrow{r} + \mu_\theta \overleftrightarrow{\theta}\overleftrightarrow{\theta} + \mu_z \overleftrightarrow{z}\overleftrightarrow{z}$, respectively, in cylindrical coordinates. The incident magnetic field is assumed to be along the z direction (the transverse-magnetic case) with time-dependence $\exp(-i\omega t)$. Then, the scattering of the cylinder is only related to ε_r, ε_θ, and μ_z. For convenience, we set $\varepsilon_t = \varepsilon_\theta = \varepsilon_z$ and $\mu_t = \mu_\theta = \mu_z$, where $\varepsilon_r(\mu_r)$ and $\varepsilon_t(\mu_t)$ stand for the permittivity (permeability)

elements corresponding to the electric and magnetic field vectors, which are normal to and tangential to the local optical axis, respectively, i.e., the constitutive tensors are diagonal in cylindrical coordinates with values $\varepsilon_r(\mu_r)$ in the radial ($\overleftrightarrow{r}$) direction and $\varepsilon_t(\mu_t)$ in the other two directions ($\overleftrightarrow{\theta}$ and $\overleftrightarrow{z}$). [21].

The wave equation is written as

$$\frac{1}{r}\left[\frac{\partial}{\partial r}\left(\frac{r}{\varepsilon_t}\frac{\partial H_z}{\partial r}\right)\right]+\frac{1}{r^2}\frac{\partial}{\partial\theta}\left(\frac{1}{\varepsilon_r}\frac{\partial H_z}{\partial\theta}\right)+k_0^2\mu_t H_z=0. \quad (1)$$

In general, the local field solutions in the inner and outer region of the wire can be described as $H_z^{\text{in}}=\sum_{m=-\infty}^{m=-1} i^m C_m J_{-m'}(kr)e^{im\theta}+\sum_{m=0}^{m=\infty} i^m D_m J_{m'}(kr)e^{im\theta}$ and $H_z^{\text{out}}=\sum_{m=-\infty}^{m=\infty} i^m[J_m(k_0 r)+B_m H_m^{(1)}(k_0 r)]e^{im\theta}$, where $k=k_0\sqrt{\varepsilon_t\mu_t}$ and $k_0=\omega\sqrt{\varepsilon_0\mu_0}$, and for the noninteger Bessel function index m', where $m'^2=m^2\varepsilon_t/\varepsilon_r$ [22]. Note that the anisotropic structure used in this Letter is different from the uniaxial material considered in Bohren's book [1]. Under TE (or TM) incidence, the uniaxial material in [1] is isotropic, while our anisotropic material is defined in a cylindrical coordinate and is not isotropic under TE (or TM) incidence. To solve the scattering problem, the scattering coefficient B_m now becomes the most important issue [22]:

$$B_m=-\frac{\sqrt{\varepsilon_t\mu_t}J'_m(q)J_{m'}(\varepsilon_t\mu_t q)-\mu_t J_m(q)J'_{m'}(\varepsilon_t\mu_t q)}{\sqrt{\varepsilon_t\mu_t}H'_m(q)J_{m'}(\varepsilon_t\mu_t q)-\mu_t H_m(q)J'_{m'}(\varepsilon_t\mu_t q)}\quad (m\geq 0), \quad (2)$$

and

$$B_m=-\frac{\sqrt{\varepsilon_t\mu_t}J'_m(q)J_{-m'}(\varepsilon_t\mu_t q)-\mu_t J_m(q)J'_{-m'}(\varepsilon_t\mu_t q)}{\sqrt{\varepsilon_t\mu_t}H'_m(q)J_{-m'}(\varepsilon_t\mu_t q)-\mu_t H_m(q)J'_{-m'}(\varepsilon_t\mu_t q)}\quad (m<0), \quad (3)$$

where the prime denotes the derivative with respect to the argument and the size parameter $q=k_0 a$.

To explain the optical resonances numerically, let us present the amplitude:

$$B_m=-\frac{\Re_m}{\Re_m+i\Im_m}, \quad (4)$$

by separating the real and imaginary parts. Due to the fact that $B_{-m}=B_m$ for $m\geq 0$, we only consider the case of $m\geq 0$. Then, we have

$$\Re_m=\sqrt{\varepsilon_t\mu_t}J_{m'}\left(\sqrt{\varepsilon_t\mu_t}q\right)J'_m(q)-\mu_t J_m(q)J'_{m'}\left(\sqrt{\varepsilon_t\mu_t}q\right), \quad (5)$$

$$\Im_m=\sqrt{\varepsilon_t\mu_t}J_{m'}\left(\sqrt{\varepsilon_t\mu_t}q\right)Y'_m(q)-\mu_t J'_{m'}\left(\sqrt{\varepsilon_t\mu_t}q\right)Y_m(q), \quad (6)$$

where Y_m is the Neumann function. The exact optical resonance corresponds to $\Im_m=0$, which leads to $|B_m|=1$. For simplicity, the material is assumed to be nonmagnetic, i.e., $\mu_t=1$.

There is only one magnetic dipole [23] resonance for $m=0$ at small q. The perturbation of anisotropic permittivity $\delta=\varepsilon_t-\varepsilon_r$ has little impact on the position of magnetic dipole resonance, and the maximum magnitude of B_0 always occurs in the vicinity of $q\cong 2.8$ (not shown here). However, the situation is different for other higher-order modes (e.g., electric dipolar $m=2$, quadrupolar $m=3$, etc.), where new resonances are excited under the resonant condition $\varepsilon_t\cdot\varepsilon_r>1$, as is shown in Figs. 1(a) and 1(b). Compared with the isotropic case, i.e., $\varepsilon_t=\varepsilon_r=-1$ (black lines), additional optical resonances emerge at very small q when the perturbation of anisotropy $\delta\neq 0$. For a small cylinder in the long-wavelength limit, the scattering coefficient B_1 has the following form:

$$B_1\approx -\pi q^2/2\left(\sqrt{\varepsilon_r}+1/\sqrt{\varepsilon_r+\delta}\right). \quad (7)$$

From the above equation, one can see that a small perturbation will lead to a small value of $\sqrt{\varepsilon_r}+1/\sqrt{\varepsilon_r+\delta}$; thus, it requires small size parameter q to achieve $|B_1|=1$. The smaller the perturbation is, the closer the resonance is to the size $q=0$. This property brings forward a new prospect of designing high-sensitivity optical devices at the scale of several nanometers. Note that $|B_1|=1$ is not a sufficient condition for the optical resonance. One could check this condition with the partial scattering cross sections $Q_{\text{sca},m}$, where m ($m=1, 2, 3\ldots$) means the scattering solely comes from mode m. As is shown in Fig. 1(c), the scattering resonances of dipole and quadrupole correspond to $|B_1|=1$ and $|B_2|=1$ at $q<1$, respectively.

Figure 1(d) shows the narrow quadrupolar resonances interacting with the broad dipolar resonance, which may produce Fano resonance. For a given size q, e.g., $q=0.3$, the distance between quadrupolar modes and dipolar modes (marked with yellow points) does not vary much for the isotropic and anisotropic cases. What is more, the position (i.e., the size q) of Fano resonance is always in the vicinity of narrow resonance. Thus, the strength of interference of these two modes remains at the same level. Note that using anisotropy particles offers an additional degree of freedom to manipulate Fano resonance. For example, for a given small size, one could tune ε_r to obtain the desired range of ε_t for Fano resonance, which is suitable to use some metals such as Au and Ag. When the particle's loss is weak, the resonances are slightly suppressed but still resemble the lossless case.

Fano resonance of individual solid structures can be observed by the differential scattering spectra, such as forward scattering (FS) or backward scattering (BS) [3,4]. In the vicinity of Fano resonance, a tiny change in anisotropy will cause dramatic variations in far-field scattering and near-field energy

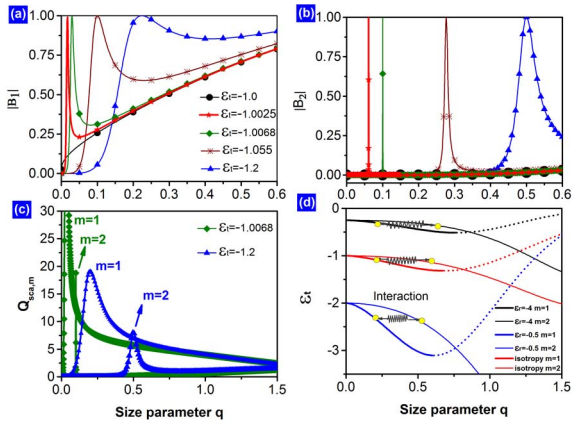

Fig. 1. Analysis of resonant conditions and dominant modes versus size parameter q for (a) dipole resonance $m=1$ and (b) quadrupole resonance $m=2$. (a), (b), and (c) New additional resonances induced by the tiny perturbation in anisotropy for high-order resonances (e.g., dipole, quadrupole, etc.) for the same $\varepsilon_r=-1$. (d) Interactions between dipole resonance and quadrupole resonance under different ε_r. Dotted lines stand for the cases that satisfy $|B_m|=1$ but do not correspond to optical resonances.

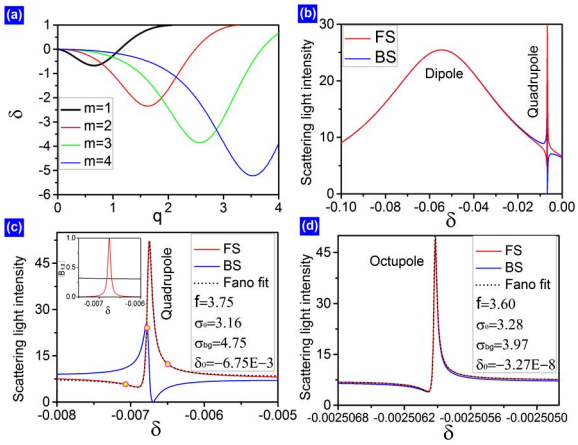

Fig. 2. Trajectories of the four first resonances B_m for $\varepsilon_r = -1$. At the size of $q = 0.1$, the corresponding anisotropy δ_m are $\delta_1 = -0.05457$, $\delta_2 = -0.00676$, $\delta_3 = -0.00251$, and $\delta_4 = -0.00133$, respectively. (b) to (d) Forward scattering and backward scattering versus anisotropy around these resonances. Typical Fano asymmetric resonances only appear for higher-order modes ($m \geq 2$). The forward-scattering resonances can be perfectly fitted by the Fano formula. Inset shows the strength of dipole (black) and quadrupole (red) modes versus permittivity anisotropy.

flow distribution. For a given particle size, further reducing the anisotropy ($|\varepsilon_t - \varepsilon_r|$) produces higher multipolar modes, which can interfere with the broad electric dipole mode generating higher-order Fano resonance, as is shown in Fig. 2. For the lowest-energy Fano resonance (origin from the constructive and destructive interference of dipole and quadrupole), the FS and BS show typical asymmetric profiles, which can be exactly fitted by the Fano formula [24]:

$$F(\tau) = \sigma_0 \frac{(\tau + f)^2}{1 + \tau^2} + \sigma_{bg}, \tag{8}$$

with $\tau = 2(\delta - \delta_0)/\Gamma$, where δ_0 and Γ are the position and width of the resonance, σ_0 and σ_{bg} are the normalized and background scattering, and f is the asymmetry parameter. For simplicity, only the Fano fit of forward scattering resonance is shown in the picture. To illustrate the interactions of dipole and quadrupole modes, we inset the strength of the two modes over anisotropy in Fig. 2(c). When the amplitudes of the dipole mode (continuum) and quadrupole mode (discrete) are at the same level, the two modes interact with each other, leading to the asymmetric profile of FS and BS.

FS and BS flip over quickly around the quadrupole resonance with anisotropy variation. The dynamic evolution of fast-switching radiation can be found in Visualization 1. On the contrary, the FS and BS in Fig. 2(d) are almost identical around the octupolar resonance, though their profiles are quite asymmetric as well. This is due to the fact that FS and BS share similar expressions around the octupolar resonance, both of which are proportional to $|b_1 + b_3|^2$. The background scattering ($\sigma_{bg} = 4.0$) of the octupole Fano resonance is close to that of quadrupole ($\sigma_{bg} = 4.8$) because they share the same broad dipole resonance. Visualization 2 demonstrates the synchronous resonance along the change of anisotropy near $\delta = -0.002506$.

In general, the interference of resonance comes from the coupling of the localized surface plasmon and incident wave. Far-field scattering and near-field energy flux can be totally reversed around the Fano resonance. Optical singularities and Fano resonance are intrinsically linked due to their identical origin of interference [2,7,25]. It is instructive to investigate the trajectory of energy flux and the topology of optical singularities. This system has two kinds of singular points: vortex and saddle points [26]. When these points get close, they could form saddle-vortex pairs and dramatically modify the power flow around them. In Fig. 3, we show the singularity distribution and streamlines of Poynting vector S, which clearly reveal the magnitude and direction of the transferring rate of electromagnetic energy [27]. Four typical situations are presented: (i) no anisotropy ($\delta = 0$), i.e., isotropy case; (ii) anisotropy case at equilibrium state of quadrupole Fano resonance; (iii) and (vi) birefringent cases "before" and "after" the equilibrium resonant state. The corresponding positions are marked with yellow dots in Fig. 2(c).

In Fig. 3(a), the Poynting vector of an isotropic case for $\varepsilon = -1$ is rather multiplicate and magnificent, due to the overlapping of multiple resonances. A unique characteristic of an isotropy cylinder is that all plasmon resonances start from the same value $\varepsilon = -1$ at small size parameter ($q \to 0$). The situation is different when anisotropy is introduced into the system. The constructive and destructive interferences of higher-order and dipole modes can result in intensive field enhancement and the flip of optical scattering. Let us take Fano resonance near a quadrupole mode for example. Figures 3(b)–3(d) and Fig. 4 show the near fields of Fano resonance and the corresponding far field scattering, respectively.

"Below" the Fano resonance (smaller anisotropy $|\delta|$ than that of equilibrium resonant state), four vortex points accompanied by two saddle points appear at the boundary of the particle. The four vortex points represent the localized quadrupole plasmon, while they are united by saddles points forming two

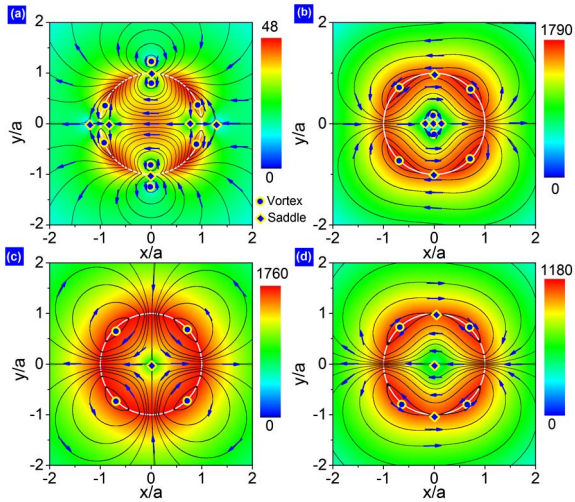

Fig. 3. Poynting vector $|\mathbf{S}|$ distribution, lines of Poynting vector $\mathbf{S}$, and singular points for (a) isotropic cylinder $\delta = 0$ and anisotropic ones (b) $\delta = -0.0065$; (c) $\delta = -0.0067835$; (d) $\delta = -0.0071$. Parameters: $q = 0.1$ and $\varepsilon_r = -1$. In the figures, two types of singularities are shown: vortex points (circles) and saddle points (squares). The cylinder is outlined in white, and the light strikes normally onto the cylinder from the right side.

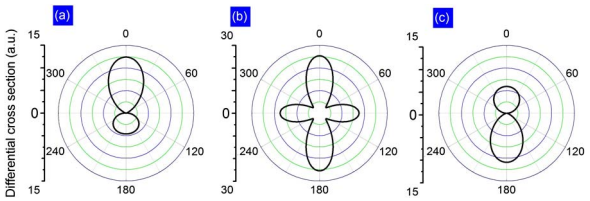

Fig. 4. Polar diagrams for light intensity versus observation angle θ associated with Fano resonance and fast-switching radiation pattern. We assume $q = 0.1$ and $\varepsilon_r = -1$. (a) $\delta = -0.0065$; (b) $\delta = -0.0067835$; (c) $\delta = -0.0071$. Light is incident from the bottom of the pictures. Switching radiation pattern versus the change of anisotropy has been demonstrated (see Visualization 1).

dipole-like vortex-saddle-vortex pairs. The localized plasmons interfere constructively with the incoming electromagnetic wave, exciting parallel energy flow to the incoming wave at the surface of the particle. The near-field Poynting lines are much like the magnetic dipole radiation by an excited metallic split-ring resonator [28]. The radiation of light is scattered mostly in the direction of wave propagation, i.e., forward scattering. The constructive interaction is reinforced with the increasing of anisotropy to the position of Fano resonance $\delta_0 = -0.00675$. After that, the particle scatters more in the longitudinal direction (the forward scattering decreases at the same time).

When the particle reaches the equilibrium resonant state (two saddle points on the boundary disappear), the energy flow distributes symmetrically around the particle, showing a typical quadrupolar pattern. The far-field scattering is also symmetrical in all directions. Beyond the equilibrium resonant state, the phase of scattered field changes by π and, thus, reverses the power flow direction of singular points around the particle. The energy flows outside the particle are antiparallel to the incident wave; then, the localized surface plasmon begins to interfere destructively with the incident light. The reversal of vortex handedness and motion of singular points lead to a path transform of energy flow in the vicinity of the particle: from pass-by to pass-through (see the animation of energy flow in Visualization 3). Below the Fano resonance, localized surface plasmons excite opposite energy flow inside the particle, and the incident light dodges past it. Above the Fano resonance, the vortex handedness around the particle is reversed, and numerous energy flows are attracted through the particle. The transition of two energy propagation paths was also observed in a photonic crystal waveguide with a coupled defect system [7]. Meanwhile, FS and BS switch rapidly as well to a tiny change in anisotropy, which could detect fine variations in plasmonic materials. With the enhancement of destructive interaction, both FS and BS drop quickly. But the FS drops faster than the BS, resulting in relatively strong BS. The reverse of energy flow direction also can be found in higher-order Fano such as octupole. However, the near-field pattern is much more complicated (with more singularity points) than the quadrupole one. The effect of fast switch in far-field scattering is neutralized or weakened, as is shown in Fig. 2(d).

In conclusion, we have proposed optical Fano resonances by anisotropy and revealed the physical mechanism of constructive and destructive interferences. The distribution of singular points and the direction of power flux around the particle can give us fresh insight on light–matter interactions. Meanwhile, Fano resonance renders nanostructures into a distinctive property; thus, small perturbations in anisotropy can induce dramatic variations in near and far fields. This inherent property is robust to loss as well. The high sensitivity can find applications in biological sensors, data storage, and optical switches.

Funding. National Natural Science Foundation of China (NSFC) (11374223, 11504252); National Basic Research Program (2012CB921501); Ph.D. Program Foundation of the Ministry of Education of China (20123201110010); Natural Science Foundation for Colleges and Universities in Jiangsu Province of China (15KJB140008); PAPD of Jiangsu Higher Education Institutions.

REFERENCES

1. C. F. Bohren and D. R. Huffman, *Absorption and Scattering of Light by Small Particles* (Wiley, 1983).
2. M. I. Tribelsky and B. S. Luk'yanchuk, Phys. Rev. Lett. **97**, 263902 (2006).
3. M. I. Tribelsky, S. Flach, A. E. Miroshnichenko, A. V. Gorbach, and Y. S. Kivshar, Phys. Rev. Lett. **100**, 043903 (2008).
4. B. Luk'yanchuk, N. I. Zheludev, S. A. Maier, N. J. Halas, P. Nordlander, H. Giessen, and C. T. Chong, Nat. Mater. **9**, 707 (2010).
5. U. Fano, Phys. Rev. **124**, 1866 (1961).
6. A. E. Miroshnichenko, S. Flach, and Y. S. Kivshar, Rev. Mod. Phys. **82**, 2257 (2010).
7. Y. Xu, A. E. Miroshnichenko, and A. S. Desyatnikov, Opt. Lett. **37**, 4985 (2012).
8. J. Butet, G. Bachelier, I. Russier Antoine, C. Jonin, E. Benichou, and P.-F. Brevet, Phys. Rev. Lett. **105**, 077401 (2010).
9. H. Chen, S. Liu, J. Zi, and Z. Lin, ACS Nano **9**, 1926 (2015).
10. Z. Li, S. Zhang, L. Tong, P. Wang, B. Dong, and H. Xu, ACS Nano **8**, 701 (2014).
11. W. S. Chang, J. B. Lassiter, P. Swanglap, H. Sobhani, S. Khatua, P. Nordlander, N. J. Halas, and S. Link, Nano Lett. **12**, 4977 (2012).
12. M. Rahmani, B. Luk'yanchuk, and M. Hong, Laser Photon. Rev. **7**, 329 (2013).
13. F. Hao, P. Nordlander, Y. Sonnefraud, P. V. Dorpe, and S. A. Maier, ACS Nano **3**, 643 (2009).
14. N. Verellen, Y. Sonnefraud, H. Sobhani, F. Hao, V. V. Moshchalkov, P. V. Dorpe, P. Nordlander, and S. A. Maier, Nano Lett. **9**, 1663 (2009).
15. F. J. Garcia-Vidal, L. Martin-Moreno, T. Ebbesen, and L. Kuipers, Rev. Mod. Phys. **82**, 729 (2010).
16. R. Singh, I. A. I. Al-Naib, Y. Yang, D. Roy Chowdhury, W. Cao, C. Rockstuhl, T. Ozaki, R. Morandotti, and W. Zhang, Appl. Phys. Lett. **99**, 201107 (2011).
17. F. Hao, Y. Sonnefraud, P. Van Dorpe, S. A. Maier, N. J. Halas, and P. Nordlander, Nano Lett. **8**, 3983 (2008).
18. C. Wu, A. B. Khanikaev, R. Adato, N. Arju, A. A. Yanik, H. Altug, and G. Shvets, Nat. Mater. **11**, 69 (2011).
19. F. Flossmann, U. T. Schwarz, M. Maier, and M. R. Dennis, Phys. Rev. Lett. **95**, 253901 (2005).
20. D. Gao, A. Novitsky, T. Zhang, F. C. Cheong, L. Gao, C. T. Lim, B. Luk'yanchuk, and C.-W. Qiu, Laser Photon. Rev. **9**, 75 (2015).
21. Q. Cheng, W. X. Jiang, and T. J. Cui, Phys. Rev. Lett. **108**, 213903 (2012).
22. H. L. Chen and L. Gao, Phys. Rev. A **86**, 033825 (2012).
23. W. Liu, A. E. Miroshnichenko, R. F. Oulton, D. N. Neshev, O. Hess, and Y. S. Kivshar, Opt. Lett. **38**, 2621 (2013).
24. A. E. Miroshnichenko, Phys. Rev. A **81**, 053818 (2010).
25. A. S. Desyatnikov, M. R. Dennis, and A. Ferrando, Phys. Rev. A **83**, 063822 (2011).
26. A. Bekshaev, K. Y. Bliokh, and M. Soskin, J. Opt. **13**, 053001 (2011).
27. L. D. Landau and E. M. Lifshitz, *Electrodynamics of Continuous Media* (Pergamon, 1984).
28. A. I. Kuznetsov, A. E. Miroshnichenko, Y. H. Fu, J. Zhang, and B. Luk'yanchuk, Sci. Rep. **2**, 492 (2012).